electronics

Article

A Reduced Sparse Dictionary Reconstruction Algorithm Based on Grid Selection

Zhiqi Gao [1,2], Caimei Zhao [1,2], Pingping Huang [1,2,*], Wei Xu [1,2] and Weixian Tan [1,2]

[1] College of Information Engineering, Inner Mongolia University of Technology, Hohhot 010080, China; gzqngd@imut.edu.cn (Z.G.); 20211800120@imut.edu.cn (C.Z.); xuwei1983@imut.edu.cn (W.X.); wxtan@imut.edu.cn (W.T.)
[2] Inner Mongolia Key Laboratory of Radar Technology and Application, Hohhot 010051, China
* Correspondence: hpp@imut.edu.cn

Abstract: A sparse dictionary reconstruction algorithm based on grid selection is introduced to solve the grid mismatch when using the sparse recovery space time adaptive processing (SR-STAP) algorithm. First, the atom most closely related to clutter is selected from the traditional dictionary through the spectral value dimensionality reduction method. The local mesh is divided around the selected atoms to create mesh cells, and the mesh cells that are most likely to appear in the real clutter points are judged according to the local selection iteration criteria. In this way, the mesh spacing is refined, the local mesh selection is carried out step by step, and the optimal atoms in the local region are constantly adjusted and selected to narrow the search region until the iteration termination condition is met. Finally, the space-time plane is divided using a novel meshing technique that centers around the optimal atom. By removing atoms beyond the maximum range of spatial and Doppler frequencies, the simplified sparse dictionary can overcome the mesh mismatch problem. The simulation results demonstrate that the algorithm enhances the sparse recovery accuracy of clutter space-time spectrum, mitigates the mesh mismatch effect, and boosts STAP performance.

Keywords: space-time adaptive processing; grid mismatch; grid selection; reduced dictionary; sparse recovery

Citation: Gao, Z.; Zhao, C.; Huang, P.; Xu, W.; Tan, W. A Reduced Sparse Dictionary Reconstruction Algorithm Based on Grid Selection. *Electronics* **2024**, *13*, 874. https://doi.org/10.3390/electronics13050874

Academic Editor: Yide Wang

Received: 16 December 2023
Revised: 8 February 2024
Accepted: 22 February 2024
Published: 24 February 2024

1. Introduction

Airborne radar enjoys widespread utilization across diverse domains, such as moving target detection and remote sensing imaging, attributed to its superior maneuverability and extensive detection capabilities. However, airborne radar faces significant clutter, which easily interferes with moving targets, thereby leading to a substantial diminution in target detection capabilities [1]. As an extension technology of array signal processing, space-time adaptive processing (STAP) technology can significantly enhance the moving target detection performance in clutter background through two-dimensional joint processing in space and time domains [2–5]. This technique integrates the space-time degrees of freedom (DOFs) to build an adaptive angle-Doppler two-dimensional filter dynamically to suppress the clutter in the range cell to be detected, which can minimize the output clutter power while maintaining the desired signal response. According to the Reed–Mallett–Brennan (RMB) rule [6], only when the number of independent and identically distributed (IID) clutter snapshots is not less than twice the number of system DOFs, the output signal-to-noise ratio loss of a filter can be guaranteed to be less than 3 dB [7]. However, in practical applications, especially under non-stationary conditions, the above requirements can be difficult to meet, and enough IID samples can be challenging to obtain. Hence, addressing the challenge of enhancing clutter suppression, especially when confronted with limited training samples, remains a pivotal concern in STAP applications.

To solve the aforementioned problem, recent research has introduced diverse methods, including the reduced-dimensional STAP method [8,9], reduced-rank STAP method [10,11], knowledge-aided STAP method [12], and sparse recovery STAP (SR-STAP) method [13]. For the reduced-dimensional and reduced-rank STAP methods, the required number of training samples can be reduced to twice the dimensionality reduction or twice the clutter rank, but in a non-uniform environment, the necessary amount of samples is still large. The knowledge-aided STAP method uses prior information, such as environmental state, radar system parameters, and platform motion parameters, to improve the STAP performance. Thus, the performance of this method greatly depends on the accuracy of prior knowledge. The SR-STAP method introduces the sparsity of clutter distribution in the space-time domain and uses norm minimization to estimate the clutter covariance matrix (CCM), which can recover a high-resolution clutter power spectrum using only a limited number of training samples and achieve an improved clutter suppression performance. According to the solution method, SR-STAP can be broadly categorized into four categories: the greedy method, convex optimization method, non-convex optimization method, and Bayesian method. A typical greedy method is an orthogonal matching pursuit algorithm [14], which uses the inner product matching criterion for atom recognition and performs Schmidt orthogonalization on the column vectors of the measurement matrix selected for each iteration. The least square method is used to obtain the coefficients of a high-dimensional signal at a non-sparse position. Because the selected column vectors are the most relevant to the current residual in each iteration, the orthogonal residual can be rapidly reduced. The convex optimization method [15] can effectively solve the sparse coefficient by constructing a sparse relaxation model and using traditional methods, such as the gradient descent method and iterative shrinkage threshold method. However, it requires setting the regularization parameters, and its performance depends on this parameter setting. Analogous to convex optimization methods, non-convex optimization methods employ approximations to reconstruct the sparse recovery problem and devise a suite of algorithms, such as the focal underdetermined system solver (FOCUSS) algorithm [16], whose space-time power spectrum resolution can be enhanced without loss of DOFs. The Bayesian methods transform the sparse recovery problem into a maximum a posteriori estimation problem and uses its mean to estimate the sparse coefficient. The sparse Bayesian learning (SBL) method is one of the representative Bayesian methods [17]. The SBL method assumes that each element in the sparse coefficient vector obeys a zero-mean Gaussian distribution with independent parameters that are called hyperparameters. The maximum likelihood estimation method is used to learn the hyperparameters' values from the observation vector to obtain a sparser solution compared to the other sparse recovery algorithms. Although the SR-STAP method can significantly reduce the requirement for the sample number to an acceptable level, in the CCM estimation, the discrete space-time grid can cause the grid mismatch problem, which can severely limit the application of the SR-STAP method in engineering.

In recent years, several algorithms have been suggested as solutions to address the grid mismatch issue in the SR-STAP methods [18–20]. A meshless method, which uses the low-rank matrix recovery theory and the atomic norm to recover clutter directly in a continuous grid, avoiding the grid mismatch problem, was proposed in [21]. A self-tuning off-grid sparse Bayesian learning STAP algorithm based on a weighted least squares update dictionary matrix, whose dictionary is updated iteratively by samples and which can reduce the influence of the grid mismatch, was proposed in [22]. A STAP algorithm with an adaptive Laplace prior was introduced in [23]; this algorithm uses a Bayesian model based on Laplace prior, and constructs a dimensionality reduction dictionary. In this method, the estimation accuracy of the CCM is improved, and the amount of calculation is reduced. In addition, a STAP algorithm for meshless sparse Bayesian learning, which uses the block-Toeplitz matrix to check and parameterize the SBL cost function, was developed. The proposed non-convex objective function was transformed by an iterative method, which alleviated the influence of the mesh mismatch problem [24]. A dictionary construction method, which represents an innovative method in space-time dictionary construction and differs from the traditional grid division method, was developed in [25]; however, this method has poor clutter suppression performance. An algorithm for finding the matching atoms using the subspace projection method and local grid segmentation was proposed in [26]; while its computational complexity is relatively low, its robustness decreases after multiple iterations. Moreover, the clutter power spectrum shows a serious broadening phenomenon, and the sparse recovery accuracy needs to be further improved.

Aiming to solve the shortcomings of the existing methods, this paper proposes a reduced sparse dictionary reconstruction algorithm based on the grid selection. The proposed algorithm first selects atoms with larger power spectrum values and then divides the surrounding space-time plane around the selected atoms and selects the grid layer by layer, constantly adjusting the location of the optimal atom until the set error allowable conditions are met. Finally, a locally reduced sparse dictionary is constructed based on the selected center. The results of simulation experiments show that the proposed algorithm can effectively overcome the problem of grid mismatch, achieve high-precision clutter power spectrum estimation, and significantly improve clutter suppression performance.

The subsequent sections of this paper are arranged in the following manner: Section 2 describes the STAP signal model of airborne radar. Section 3 explains the SR-STAP principle and the grid mismatch problem. Section 4 details the suggested sparse dictionary reconstruction algorithm that is founded upon grid selection. Section 5 carries on the experimental analysis of the algorithm, and Section 6 summarizes the full text.

2. Signal Model

Think of an airborne side-looking uniform linear array radar consisting of N array elements, where the array element spacing d is half of the operational wavelength of the radar. The carrier platform's altitude is denoted as H, the pulse repetition frequency is given as f_r, and the number of pulses within a coherent processing interval (CPI) is designated as M. The geometric model of this airborne radar is shown in Figure 1, where V_a is the speed of the carrier platform moving along the x-axis direction, and α and θ are the pitch angles of the ground reflection point and azimuth, respectively.

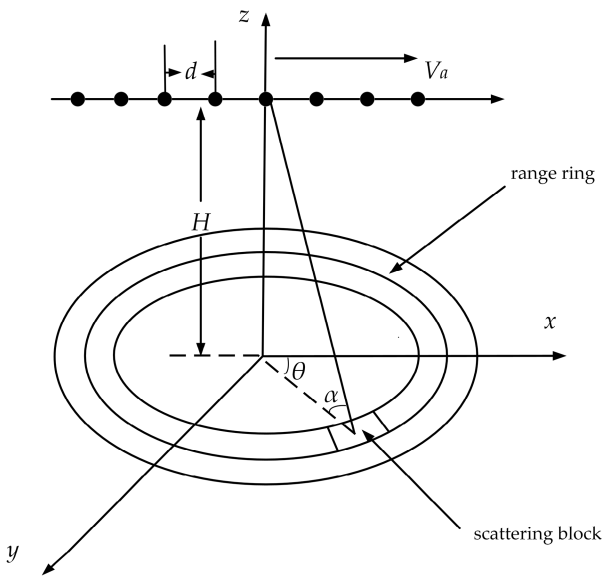

Figure 1. Airborne radar geometry model.

Ignoring the impact of range ambiguity, clutter-plus-noise space-time snapshot data obtained from a range cell can be expressed as follows:

$$\boldsymbol{X}_c = \sum_{i=1}^{N_c} \delta_i \boldsymbol{V}(f_{d,i}, f_{s,i}) + \boldsymbol{N}, \tag{1}$$

where N_c is the number of clutter scattering blocks evenly divided along a range cell; $\boldsymbol{N} \in \boldsymbol{C}^{NM\times 1}$ is the thermal noise; δ_i is the echo complex amplitude corresponding to the ith clutter scattering block; and $\boldsymbol{V}(f_{d,i}, f_{s,i})$ is the space-time steering vector that is defined as follows:

$$\boldsymbol{V}(f_{d,i}, f_{s,i}) = \boldsymbol{V}_t(f_{d,i}) \otimes \boldsymbol{V}_s(f_{s,i}), \tag{2}$$

where

$$\boldsymbol{V}_t(f_{d,i}) = \left[1, \mathrm{e}^{\mathrm{j}2\pi f_{d,i}}, \cdots, \mathrm{e}^{\mathrm{j}2\pi(M-1)f_{d,i}}\right]^{\mathrm{T}}, \tag{3}$$

$$\boldsymbol{V}_s(f_{s,i}) = \left[1, \mathrm{e}^{\mathrm{j}2\pi f_{s,i}}, \cdots, \mathrm{e}^{\mathrm{j}2\pi(N-1)f_{s,i}}\right]^{\mathrm{T}}, \tag{4}$$

where $\otimes$ denotes the Kronecker product operation; $[\cdot]^{\mathrm{T}}$ is the transpose operation; $\boldsymbol{V}_t(f_{d,i})$ and $\boldsymbol{V}_s(f_{s,i})$ are the time steering vector and the space steering vector, respectively; $f_{d,i}$ and $f_{s,i}$ are the normalized Doppler frequency and spatial frequency of the ith clutter reflection point, respectively, which can be expressed as follows:

$$f_{d,i} = \frac{2V_a}{\lambda f_r} \cos\alpha_i \cos\theta_i, \tag{5}$$

$$f_{s,i} = \frac{d}{\lambda} \cos\alpha_i \cos\theta_i. \tag{6}$$

where, λ is the working wavelength of the radar.

Assuming that the snapshot data of each range cell are independent of each other, the CCM can be expressed as follows [27]:

$$\boldsymbol{R}_c = \mathrm{E}\left[\boldsymbol{X}_c \boldsymbol{X}_c{}^{\mathrm{H}}\right], \tag{7}$$

where $\mathrm{E}[\cdot]$ denotes the mathematical expectation operation, and $[\cdot]^{\mathrm{H}}$ is the conjugate transpose operation.

Based on the linearly constrained minimum variance (LCMV) criterion, the optimal STAP weight vector can be represented in the following manner [28]:

$$\boldsymbol{w}_{\mathrm{OPT}} = \gamma \boldsymbol{R}_c^{-1} \boldsymbol{V}_{\mathrm{target}}, \tag{8}$$

where $\boldsymbol{V}_{\mathrm{target}}$ is the space-time steering vector of a target, and $\gamma = (\boldsymbol{V}_{\mathrm{target}}{}^{\mathrm{H}} \boldsymbol{R}_c{}^{-1} \boldsymbol{V}_{\mathrm{target}})^{-1}$ is used to ensure that the filtering weight vector has a unit response to the target space-time steering vector.

Finally, the snapshot data from the detected range cell are filtered, which yields

$$\boldsymbol{y} = \boldsymbol{w}_{\mathrm{OPT}}{}^{\mathrm{H}} \boldsymbol{X}_c, \tag{9}$$

where $\boldsymbol{X}_c$ represents the snapshot data corresponding to the range cell under detection.

3. Sparse Recovery Principle and Grid Mismatch Problem

3.1. Sparse Recovery Principle

According to the existing research results, there is a coupling relationship between the spatial frequency and the Doppler frequency of clutter [29], so the clutter spectrum is sparsely distributed on the angle-Doppler plane. Considering the sparsity of the clutter distribution, the sparse recovery technique, namely the SR-STAP, can be used for clutter signal processing. First, the space-time two-dimensional plane is uniformly discretized into $G_d \times G_s$ ($G_d = \mu_d N$, $G_s = \mu_s M$) quantization units (μ_d and μ_s are the grid resolution factors, and typically $\mu_d > 1$ and $\mu_s > 1$). Therefore, the clutter snapshot data in Equation (1) can be re-expressed as follows:

$$\boldsymbol{X}_c = \sum_{m=1}^{G_d} \sum_{n=1}^{G_s} \delta_{m,n} \boldsymbol{V}(f_{d,i}, f_{s,i}) + \boldsymbol{N} = \boldsymbol{\Phi}\boldsymbol{\delta} + \boldsymbol{N}, \tag{10}$$

where $\boldsymbol{\Phi}$ is the space-time steering vector dictionary matrix with a dimension of $NM \times G_d G_s$, $\boldsymbol{\delta}$ is the sparse coefficient vector to be solved, and they are, respectively, expressed as follows:

$$\boldsymbol{\Phi} = \left[\boldsymbol{V}(f_{d,1}, f_{s,1}), \cdots, \boldsymbol{V}(f_{d,1}, f_{s,G_s}), \cdots, \boldsymbol{V}(f_{d,G_d}, f_{s,1}), \cdots, \boldsymbol{V}(f_{d,G_d}, f_{s,G_s})\right] \in \mathbf{C}^{NM \times G_d G_s} \tag{11}$$

$$\boldsymbol{\delta} = [\delta_1, \delta_2, \cdots, \delta_{G_d G_s}]^{\mathrm{T}} \in \mathbf{C}^{G_d G_s \times 1}. \tag{12}$$

Next, Equation (7) can be re-expressed as follows:

$$\boldsymbol{R}_c = \mathrm{E}\left[\boldsymbol{X_c} X_c{}^{\mathrm{H}}\right] = \boldsymbol{\Phi}\boldsymbol{P}\boldsymbol{\Phi}^{\mathrm{H}} + \sigma_n{}^2 \boldsymbol{I}_{NM} \in \mathbf{C}^{NM \times NM}, \tag{13}$$

where $\sigma_n{}^2$ is the noise power; $\boldsymbol{I}_{NM}$ is the unit matrix with a dimension of $NM \times NM$; $\boldsymbol{P} = diag(\boldsymbol{p}) \in \mathbf{C}^{G_d G_s \times G_s G_d}$ is a diagonal matrix, whose nonzero elements on the diagonal; $\boldsymbol{p} = [p_{1,1}, \ldots, p_{1,G_s}, \ldots, p_{G_d,1}, \ldots, p_{G_d,G_s}]^{\mathrm{T}} \in \mathbf{C}^{G_d G_s \times 1}$ represent the power of the clutter at different angles and Doppler frequencies, and $\boldsymbol{p}_{m,n}$= E[$|\delta_{m,n}|^2$], m = 1, 2, . . ., G_d, and n = 1, 2, . . ., G_s.

The key task in the SR-STAP method is the estimation of the clutter space-time power spectrum $\boldsymbol{p}$. The single measurement vector (SMV) method and the multiple measurement vector (MMV) method can be used to solve the space-time power spectrum [30]. The SMV method recovers $\boldsymbol{\delta}$ from data on the range cell to be detected and calculates the space-time power spectrum $\boldsymbol{p}$, which can be expressed as follows:

$$\underset{\delta}{\operatorname{argmin}} \|\boldsymbol{\delta}\|_0 \quad s.t.\ \|\boldsymbol{X}_c - \boldsymbol{\Phi}\boldsymbol{\delta}\|_2 \leq \eta, \tag{14}$$

where $\|\cdot\|_0$ and $\|\cdot\|_2$ represent the l_0 and l_2 norms of a vector, respectively, and η is the noise-allowed error.

Equation (14) represents a nondeterministic polynomial-time hard problem, and it can be transformed into an equivalent l_1 norm problem to obtain a sparse solution as follows:

$$\min_{\delta} \|\boldsymbol{\delta}\|_1 \quad s.t.\ \|\boldsymbol{X}_c - \boldsymbol{\Phi}\boldsymbol{\delta}\|_2{}^2 \leq \eta, \tag{15}$$

where $\|\cdot\|_1$ denotes the l_1 norm.

After obtaining the sparse solution, the clutter space-time spectrum can be derived as follows:

$$\boldsymbol{p} = \boldsymbol{\delta} \odot \boldsymbol{\delta}^*, \tag{16}$$

where $\odot$ represents the Hadamard product, and $[\cdot]^*$ is a complex conjugate operation.

Because a single sample contains less clutter information, the sparse recovery effect and the clutter suppression ability of the clutter space-time spectrum are poor when the signal-to-noise ratio is low or the target motion speed is slow. Generally, the MMV method can recover the clutter space-time spectrum $\boldsymbol{p}$ from multiple training samples and estimate the CCM. Assuming that the training samples satisfy the IID condition, the implementation of the MMV method can be conducted as follows:

$$\underset{p}{\operatorname{argmin}} \|\boldsymbol{p}\|_0 \quad s.t.\ \left\|\boldsymbol{R}_c - \hat{\boldsymbol{R}}_0\right\|_F{}^2 \leq \eta, \tag{17}$$

where $\|\cdot\|_F$ represents the Frobenius norm of a matrix, and $\hat{\boldsymbol{R}}_0 = \frac{1}{L}\sum_{i}^{L} x_i x_i^{\mathrm{H}}$ is the estimated CCM obtained by the traditional sample matrix inversion (SMI) [31].

The MMV method can make full use of a massive clutter sample of data, perform more robust clutter space-time spectrum recovery, and achieve clutter suppression capabilities than the SMV method.

3.2. Grid Mismatch Problem

The SR-STAP algorithm requires discretizing the continuous space-time plane. The discrete intervals of the spatial and Doppler frequencies are denoted by Δf_s and Δf_d, respectively, and the space-time plane is divided into several grids. The SR-STAP algorithm considers that the clutter is distributed on several grids on the discretized space-time plane. According to Equation (15), the clutter amplitude at the relevant grid points can be obtained, and then the sparse reconstruction of the clutter can be realized. Because real clutter is continuously distributed, and due to the influence of the noise and system parameter error on the received signal of radar, there will be a certain deviation between the real clutter point and the discrete grid point, which is called the grid mismatch. Therefore, the estimation of the sparse representation coefficient of clutter in the case of a fixed grid can introduce an obvious calculation error, which can severely degrade the STAP performance.

In the side-looking case, when the ratio of G_d and G_s is an integer multiple of the clutter ridge slope, the clutter ridge is distributed at uniform discrete grid points, and there is no grid mismatch problem; otherwise, the grid mismatch problem will appear. Figure 2a,b show the clutter distribution diagrams without and with grid mismatch, respectively. The problem of grid mismatch can lead to a decrease in the CCM estimation accuracy [32], which can further lead to a decrease in the STAP clutter suppression performance. Therefore, it is necessary to propose a new method to solve this problem.

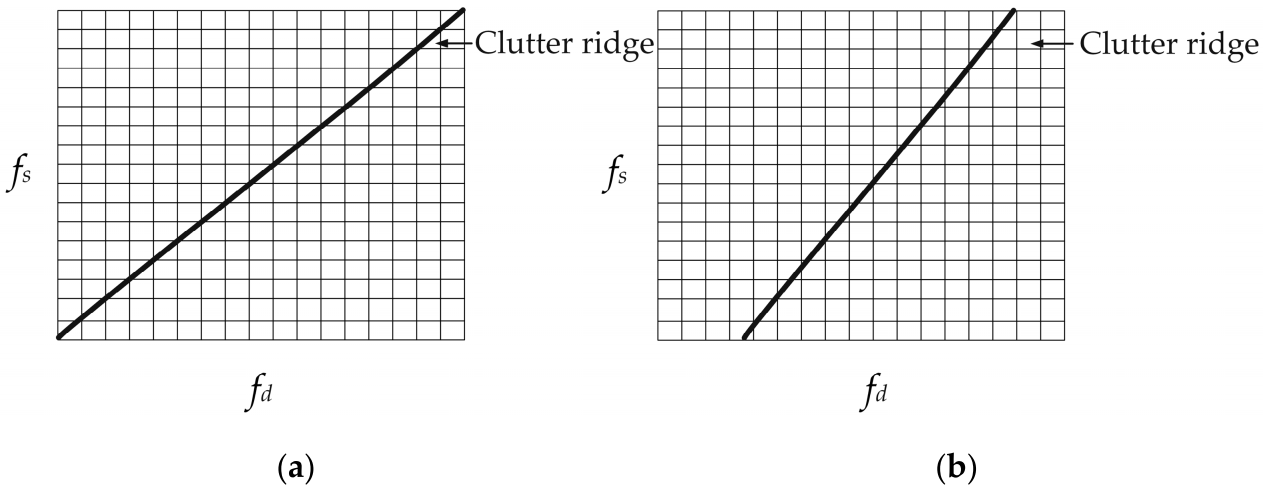

Figure 2. Discrete space-time plane clutter layouts. (**a**) On-grid clutter distribution map; (**b**) off-grid clutter distribution map.

4. Discussion Reduced Sparse Dictionary Reconstruction Algorithm Based on Grid Selection

Based on existing research results, in the SR-STAP method, the clutter covariance matrix can be estimated using only a limited number of snapshots. However, in a uniform discretization of a space-time plane, the grid mismatch problem can reduce the accuracy of the CCM estimation. To solve this problem, the study proposes a reduced sparse dictionary reconstruction algorithm based on the grid selection named the GS-SR-STAP algorithm.

4.1. Global Dictionary Construction

Assume that the space-time plane is uniformly discretized into $G_d \times G_s$ grid points, as shown in Figure 3. The Doppler frequency axis is evenly divided into G_d points with an interval of $\Delta f_d = 1/G_d$, forming the vector $[f_{s,1}, f_{s,2}, \cdots, f_{d,Gd}]$. The spatial frequency axis is evenly divided into G_s points with an interval of $\Delta f_s = 1/G_s$, forming the vector $[f_{s,1}, f_{s,2}, \cdots, f_{s,Gs}]$. Each grid point corresponds to a set of the Doppler and spatial frequencies, which are substituted into Equations (2)–(4) to obtain the space-time steering vector and construct the original dictionary $\boldsymbol{\Phi}$. Then, using the principle that the power spectrum value of a clutter point is large, atoms in the original dictionary $\boldsymbol{\Phi}$ are iteratively calculated as follows:

$$\boldsymbol{P}_{\text{capon}} = \frac{1}{\left|\boldsymbol{V}^{\text{H}}(f_{d,i}, f_{s,i})\hat{\boldsymbol{R}}^{-1}\boldsymbol{V}(f_{d,i}, f_{s,i})\right|}, \quad (18)$$

where $\hat{\boldsymbol{R}}$ is the estimation of the initial clutter covariance matrix.

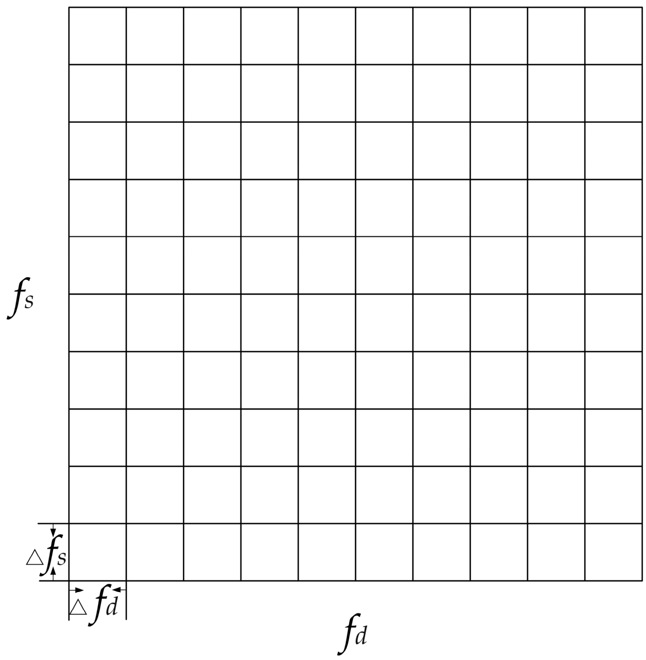

Figure 3. The original dictionary.

The calculation results of Equation (18) are sorted and numbered in descending order according to the numerical value. The first K numbers are used to select the associated space-time steering vectors for constructing the global dictionary $\boldsymbol{\Psi}_V$, first K numbers are selected to construct the global dictionary $\boldsymbol{\Psi}_V$, and the Doppler and spatial frequencies corresponding to the atoms in this dictionary are stored in a set U_0 in turn. In essence, this process is to preliminarily select the space-time steering vector most related to the real clutter which lays a foundation for the subsequent sparse dictionary construction.

4.2. Local Reduction Dictionary Construction

As mentioned above, when the global dictionary is constructed using Equation (18), only selecting appropriate atoms from the original dictionary cannot solve the problem of grid mismatch. Therefore, to obtain accurate positions of clutter points on the discretized space-time plane, the proposed GS-SR-STAP algorithm performs the local search on the area where the preliminary selected clutter points are located. A local reduction dictionary is constructed by dividing the grid along the parallel and vertical directions of the clutter ridge, thus obtaining accurate steering vectors of clutter points and estimating the clutter power spectrum more accurately. Based on this, the CCM is recalculated to enhance the performance of clutter suppression, particularly in scenarios where grid mismatch occurs.

The specific steps of the GS-SR-STAP algorithm are as follows.

STEP 1: Local grid selection

First grid selection: The ith atom in a matrix U_0 is selected and used as a center point. The spatial frequency interval $\Delta f_s/2$ ($\Delta f_s = 1/N$) and the Doppler frequency interval $\Delta f_d/2$ ($\Delta f_d = 1/M$) are used to divide the angle-Doppler plane to form a 2×2 grid, as shown in Figure 4. A total of nine grid points correspond to nine new atoms. Each atom can obtain its steering vector according to its corresponding Doppler and spatial frequencies. Then, the local optimization criterion [32] is used to select atoms as follows:

$$u_k{}^* = \underset{u \notin v^{\mathrm{k}-1}}{\arg\max} \frac{\left| \boldsymbol{V}_u{}^{\mathrm{H}} \boldsymbol{T}_n{}^{(k-1)} \hat{\boldsymbol{R}}_{\mathrm{SCM}} \boldsymbol{T}_n{}^{(k-1)} \boldsymbol{V}_u \right|}{\left| \boldsymbol{V}_u{}^{\mathrm{H}} \boldsymbol{T}_n{}^{(\mathrm{k}-1)} \boldsymbol{V}_u \right|}, \tag{19}$$

where $\boldsymbol{v}$ is the index set for storing the nine atomic numbers; $\boldsymbol{T}_n$ is the orthogonal projection matrix on the noise subspace; $\boldsymbol{V}_u$ is the space-time steering vector corresponding to a clutter atom u; $\hat{\boldsymbol{R}}_{\mathrm{SCM}} = \frac{1}{L} \sum_{l=0}^{L} \boldsymbol{X}_l \boldsymbol{X}_l^{\mathrm{H}}$ represents the CCM estimated by L training snapshots; and $\boldsymbol{T}_n{}^{k-1} \hat{\boldsymbol{R}}_{\mathrm{SCM}} \boldsymbol{T}_n{}^{k-1}$ is the residual of $\hat{\boldsymbol{R}}_{\mathrm{SCM}}$ in the kth iteration.

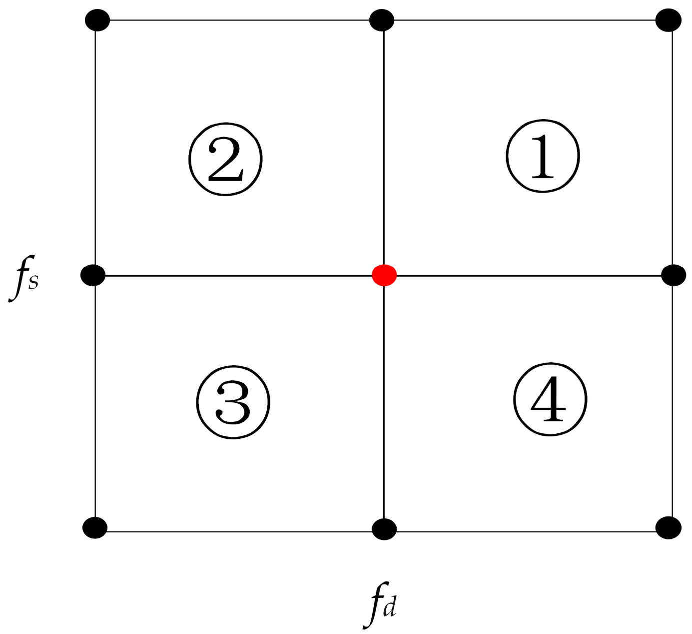

Figure 4. Grid unit diagram.

The molecule in Equation (19) represents the response of $\boldsymbol{V}_u$ to the residual, and the denominator can be regarded as the normalization of the molecule. This means that if the calculation result of Equation (19) is relatively large, the current atom must be in the clutter subspace. Thus, atoms in the initialization dictionary can be iterated according to Equation (19), and the results can be arranged in descending order and numbered in turn. Finally, the atoms corresponding to the first three numbers are selected. The number 1 atom can be used to lock the approximate position of the next layer of local division. The number 2 and number 3 atoms can assist the number 1 atom to determine the range of the next layer of local division, so that the adapted clutter atom can be quickly found.

The 2×2 grid is divided into grid cells according to the quadrant division rule, and the four quadrants correspond to four grid cells respectively. As shown in Figure 4, ① represents the first grid cell, ② represents the second grid cell, ③ represents the third grid cell, ④ represents the fourth grid cell, and then determines the grid cell where the number 1 atom, the number 2 atom, and the number 3 atom are located.

First, the region where number 1 atom is located is determined; it can fall at any of the nine grid points. If it falls at the junction of the two grid units, the auxiliary selection of atoms numbered 2 and 3 is required. Only when the three atoms fall in a grid cell, the region of the next local division can be determined. This situation can be divided into four cases, as shown in Figure 5(1)–(4). In Figure 5, the red dots represent the number 1 atom, the green dots represent the number 2 atom, and the pink dots represent the number 3 atom. The grid area surrounded by the red rectangular frame is the area of the next local division. where the red dot represents the number 1 atom, the green dot represents the number 2 atom, and the pink dot represents the number 3 atom. The grid area circled by the red rectangle box is the area divided by the next expansion locale. The distance indicated by the arrow is the length of the frequency interval.

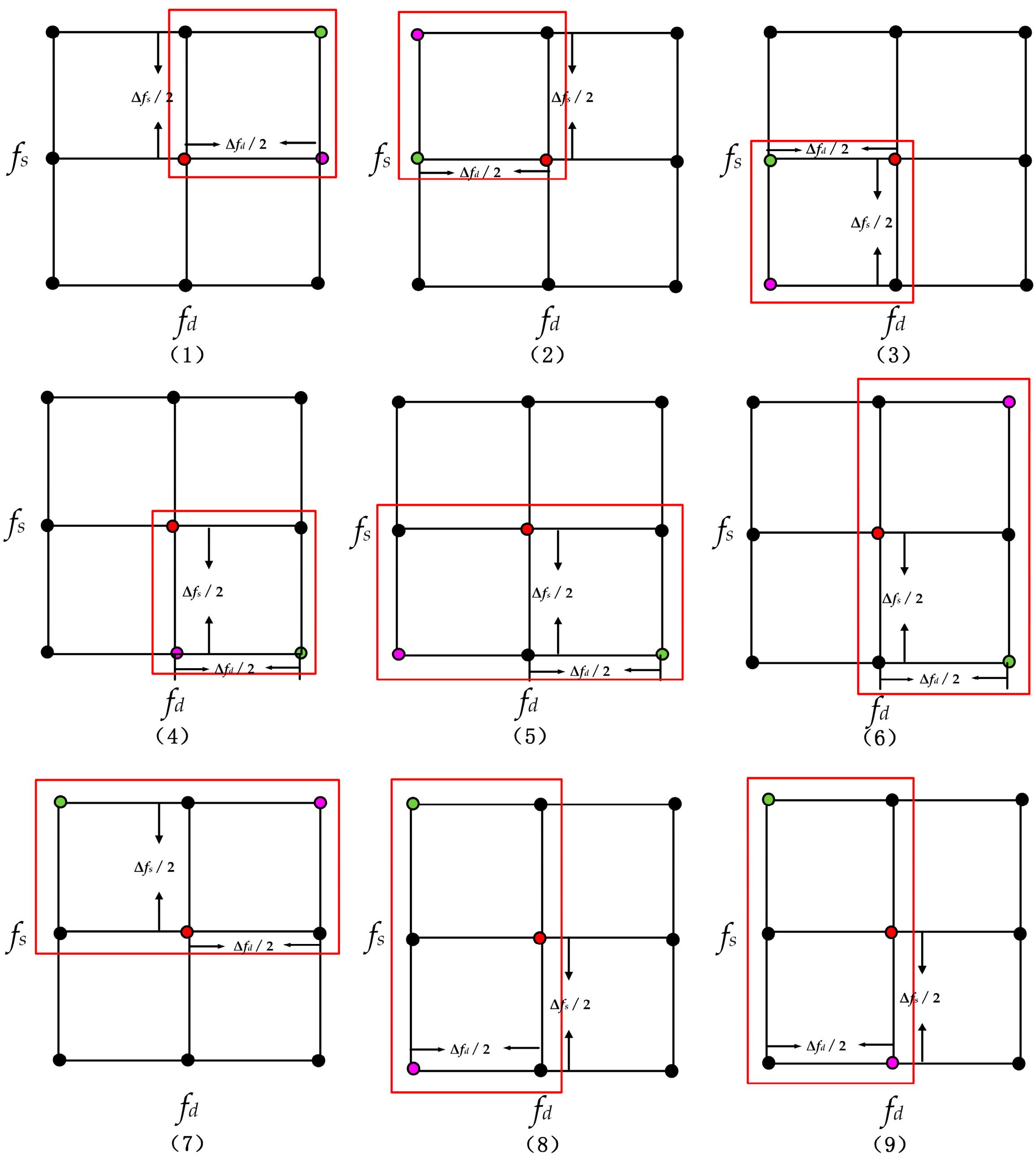

Figure 5. The first grid selection.

However, during the implementation process of the GS-SR-STAP algorithm, the atoms numbered 1–3 may not necessarily be in the same grid cell. Therefore, it is necessary to consider several cases, as shown in Figure 5(5)–(9). Atoms numbered 2 and 3 atoms may be located in two different grid cells and may form a new grid cell with number 1 atom.

Second grid selection: The grid element determined in the previous step is re-divided into the current area with a spatial frequency interval of $\Delta f_s/4$ and a Doppler frequency interval of $\Delta f_d/4$ to form a 2×2 grid, as shown in Figure 6.

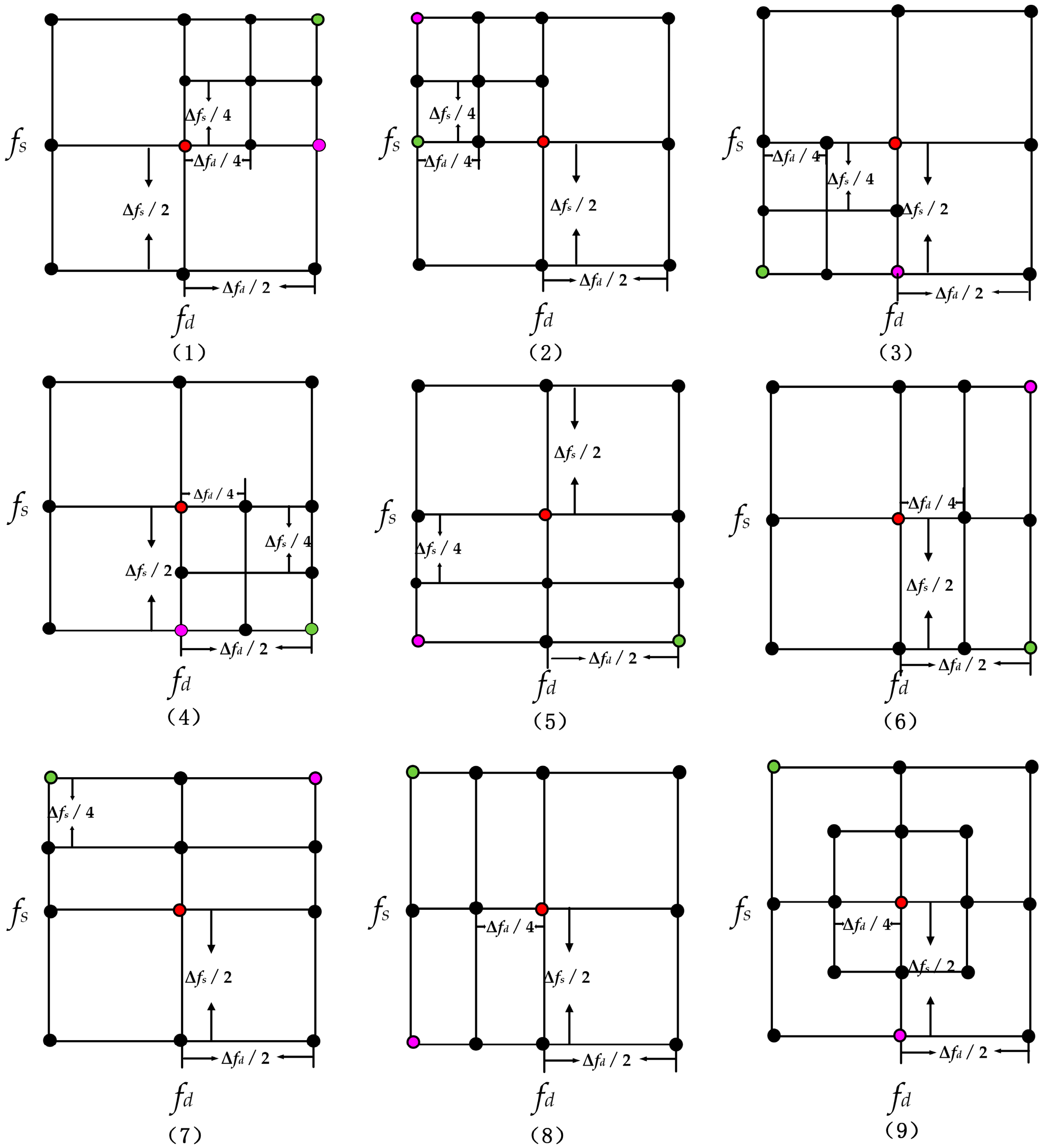

Figure 6. The second grid selection.

Equation (19) is used to calculate the power spectrum values of the atoms at each grid point, and the top three atoms with the largest power spectrum values are selected in descending order to obtain the region for the next expansion of the local division.

Third grid selection: Continue dividing the grid cells determined in the previous step into the current area with a spatial frequency interval of $\Delta f_s/8$ and a Doppler frequency interval of $\Delta f_d/8$ to form a 2×2 grid, as shown in Figure 7. The power spectrum values of atoms at each grid point are calculated using Equation (19), and three atoms with the largest power spectrum values are selected in descending order.

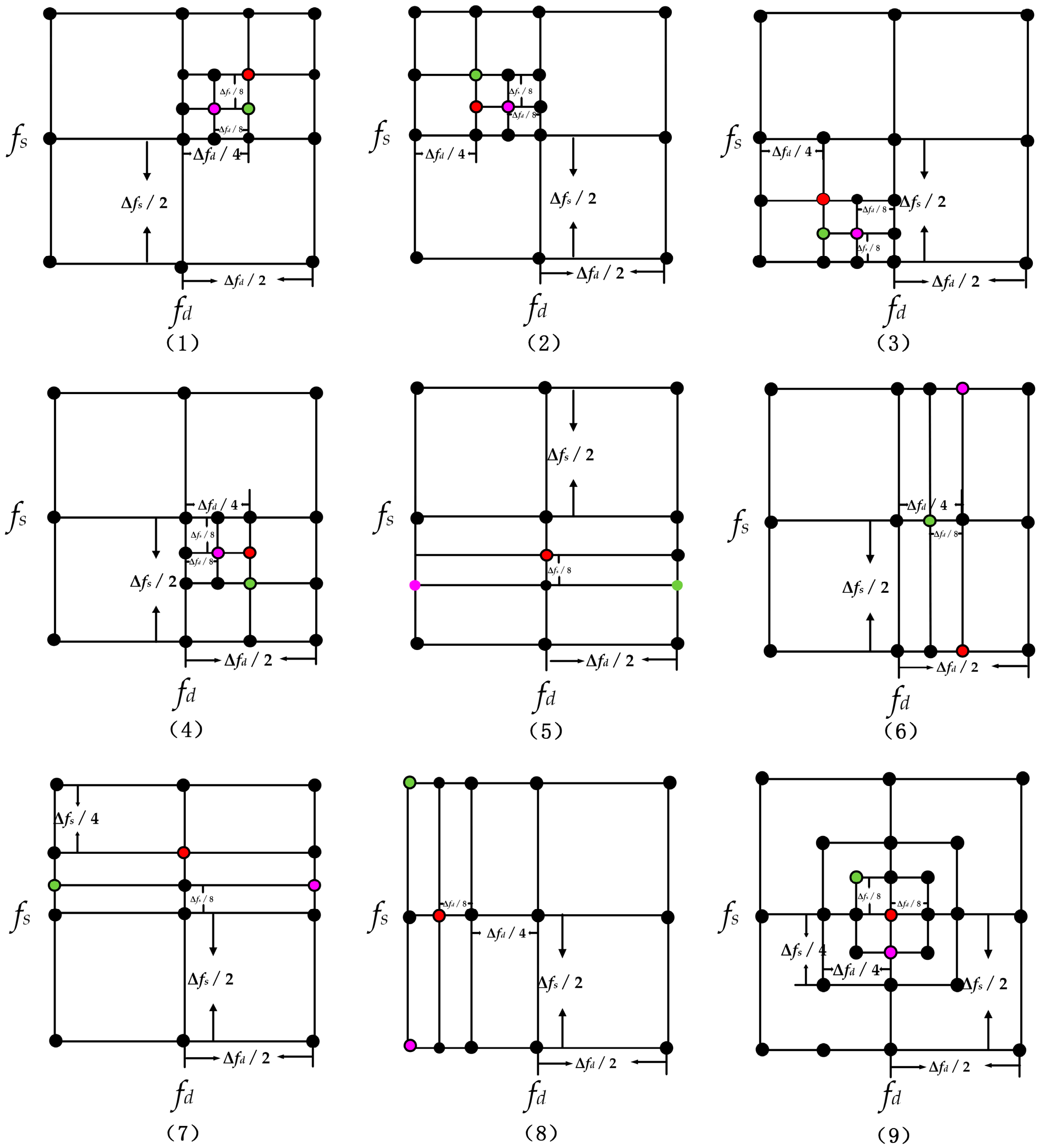

Figure 7. The third grid selection.

By analogy, the jth local area grid selection is performed in a step-by-step manner, and atom $\boldsymbol{\psi_i}^{j}$ with the largest response value is obtained until the following condition is satisfied:

$$\left\| \boldsymbol{\psi}_i{}^{(j)} - \boldsymbol{\psi}_i{}^{(j-1)} \right\|_1 < \sigma, \tag{20}$$

where σ is the allowable error threshold.

The number of the optimal atom is extracted, and the corresponding Doppler frequency f_{d_opt} and spatial frequency f_{s_opt} are found in the Doppler frequency set and spatial frequency set, respectively, by using this number.

STEP 2: Local dictionary construction

Using the Doppler and spatial frequencies determined in STEP 1 as a center, the grid is divided along the parallel and vertical directions of the clutter ridge, as shown in Figure 8. The number of grids in the parallel direction of the clutter ridge is L_1 and that in the vertical direction of the clutter ridge is L_2. The basis vector of the clutter ridge is $\boldsymbol{p}$, and the vertical direction is $\boldsymbol{q}$. Then, by combining different multiples of $\boldsymbol{p}$ and $\boldsymbol{q}$, the coordinate values of atoms in the sparse dictionary can be obtained.

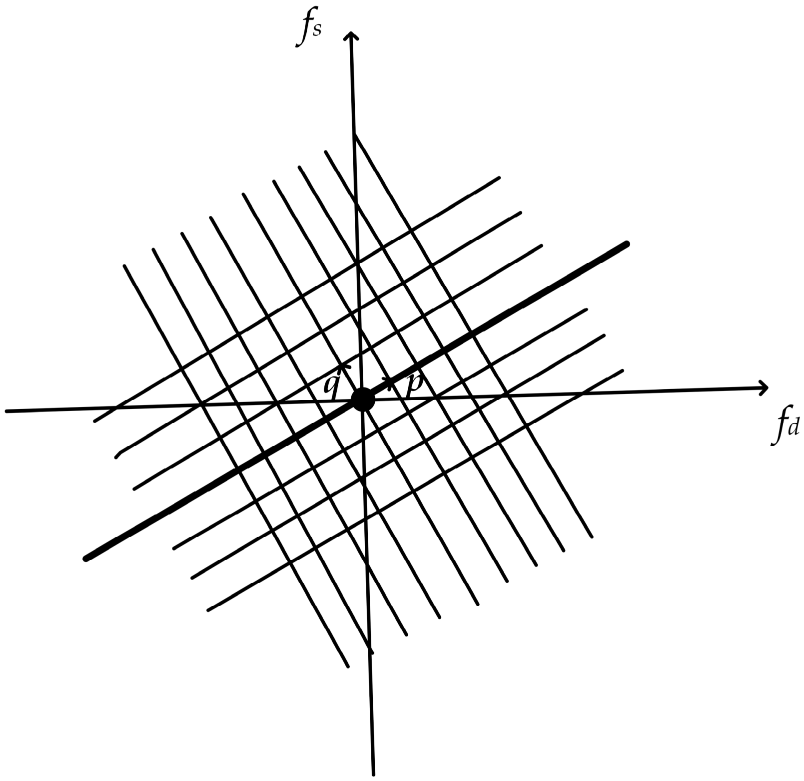

Figure 8. Schematic diagram of the local dictionary construction process.

Consider the values of length t_1 and width t_2 of a single mesh, which are also called the modulus of $\boldsymbol{p}$ and $\boldsymbol{q}$, respectively, and they are expressed as follows:

$$\boldsymbol{p} = t_1\left(\frac{1}{\sqrt{1+\beta^2}}\right) \cdot (\beta, 1), \tag{21}$$

$$\boldsymbol{q} = t_2\left(\frac{1}{\sqrt{1+\beta^2}}\right) \cdot (1, -\beta). \tag{22}$$

The folding coefficient β can be calculated using the radar system parameters as follows:

$$\beta = \frac{2V_a}{df_r}. \tag{23}$$

Next, by assuming that the total length of the clutter ridge is $t_{\max}$, it holds that

$$t_{\max} = \sqrt{(2d/\lambda)^2 + [4V/(\lambda f_r)]^2}. \tag{24}$$

Then, the values of t_1 and t_2 can, respectively, be obtained as follows:

$$\begin{array}{l} t_1 = t_{\max}/L_1 \\ t_2 = t_{\max}/L_2 \end{array}. \tag{25}$$

Combining different values of $\boldsymbol{p}$ and $\boldsymbol{q}$ generates multiple vectors, and these can subsequently be represented as follows:

$$m \cdot \boldsymbol{p} + n \cdot \boldsymbol{q}, \tag{26}$$

where $m = 0, \pm 1, \ldots, \pm L_1/2$, $n = 0, \pm 1, \ldots, \pm L_2/2$. Then, f_d and f_s corresponding to the vector $(m \cdot \boldsymbol{p} + n \cdot \boldsymbol{q})$ are expressed as follows:

$$\begin{aligned} f_d &= (mt_1\beta + nt_2)/\frac{1}{\sqrt{1+\beta^2}} \\ f_s &= (mt_1 - nt_2\beta)/\frac{1}{\sqrt{1+\beta^2}} \end{aligned} . \tag{27}$$

Therefore, the space-time two-dimensional coordinates of atoms in the sparse dictionary can be obtained as follows:

$$(f_d, f_s) = \frac{1}{\sqrt{1+\beta^2}}(mt_1\beta + nt_2, mt_1 - nt_2\beta). \tag{28}$$

When m and n are taken over all values, the value range of the spatial and Doppler frequencies of the sparse dictionary used in this study will certainly exceed the frequency value range of the original dictionary, and the excessive range of the frequency value can reduce the performance of the sparse recovery algorithm. Therefore, it is necessary to reduce the dimension of the sparse dictionary, remove a part of the spatial and Doppler frequencies, and take only the frequency within the spatial and Doppler frequencies' value range that can cover the entire clutter ridge.

The spatial frequency range of the sparse dictionary should satisfy the two following conditions:

$$\begin{cases} f_{\text{s\_min}} = f_{\text{s\_opt}} - \frac{\sqrt{2}}{2}t_1\left(\frac{L_1}{2}\right) \\ f_{\text{s\_max}} = f_{\text{s\_opt}} + \frac{\sqrt{2}}{2}t_1\left(\frac{L_1}{2}\right) \end{cases}. \tag{29}$$

Similarly, the Doppler frequency range of the sparse dictionary should satisfy the following conditions:

$$\begin{cases} f_{\text{d\_min}} = f_{\text{d\_opt}} - \frac{\sqrt{2}}{2}t_2\left(\frac{L_2}{2}\right) \\ f_{\text{d\_max}} = f_{\text{d\_opt}} + \frac{\sqrt{2}}{2}t_2\left(\frac{L_2}{2}\right) \end{cases}. \tag{30}$$

The atoms of the space-time two-dimensional coordinates calculated using Equation (27) satisfying Equations (28) and (29) are used to form a new dictionary, which can be expressed as follows:

$$\begin{cases} f_{\text{s\_min}} \le f_s \le f_{\text{s\_max}} \\ f_{\text{d\_min}} \le f_d \le f_{\text{d\_max}} \end{cases}. \tag{31}$$

By reducing the dictionary dimension, the spatial and Doppler frequencies' range in the dictionary cannot exceed those of the original dictionary to enhance the precision of sparse recovery.

The pseudo-code of the GS-SR-STAP algorithm is shown in Algorithm 1.

Algorithm 1. GS-SR-STAP algorithm.

Input: $\boldsymbol{\Psi}_V$, U_0, $\hat{\boldsymbol{R}}$

Initialization: $\boldsymbol{\Psi}_V = \{\ \}$, $\boldsymbol{v} = \{\ \}$, $U_0 = \{\ \}$, $\boldsymbol{T}_n{}^0 = \boldsymbol{I}$, $k = 1$

The first step: Global dictionary construction

Use $\boldsymbol{P}_{\text{capon}} = \frac{1}{\left|\boldsymbol{V}^{\text{H}}(f_{d,i}, f_{s,i})\hat{\boldsymbol{R}}^{-1}\boldsymbol{V}(f_{d,i}, f_{s,i})\right|}$ to construct a global dictionary

The second step: Local grid selection

The first grid selection:

Adopting the local optimization criterion

$$u_k{}^* = \underset{u \notin \boldsymbol{v}^{\text{k}-1}}{\arg\max} \frac{\left|\boldsymbol{V}_u{}^{\text{H}}\boldsymbol{T}_n{}^{(k-1)}\hat{\boldsymbol{R}}_{SCM}\boldsymbol{T}_n{}^{(k-1)}\boldsymbol{V}_u\right|}{\left|\boldsymbol{V}_u{}^{\text{H}}\boldsymbol{T}_n{}^{(\text{k}-1)}\boldsymbol{V}_u\right|},$$

three atoms with the largest power spectrum values in the current region are selected to narrow the local search range;

The second grid selection:

Using the above formula, the three atoms with larger power spectral values in the current region are further screened out.

The jth local partition:

Repeat the previous step until atom $\boldsymbol{\psi}_i{}^j$ with the largest power spectrum value satisfies the condition of $\left\|\boldsymbol{\psi}_i{}^{(j)} - \boldsymbol{\psi}_i{}^{(j-1)}\right\|_1 < \sigma$, and determine the Doppler frequency $f_{\text{d\_opt}}$ and the spatial frequency $f_{\text{s\_opt}}$ corresponding to atom $\boldsymbol{\psi}_i{}^j$.

The third step: Local reduction dictionary construction

The space-time plane is divided by a method of dividing the grid along the clutter ridge direction and the vertical direction of the clutter ridge.

$\beta = \frac{2V_a}{df_r}$

$(f_d, f_s) = \frac{1}{\sqrt{1+\beta^2}}(mt_1\beta + nt_2, mt_1 - nt_2\beta)$,

$m = 0, +1, \ldots, +L_1/2,\ n = 0, +1, \ldots, +L_2/2$

$f_{\text{d\_min}} = f_{\text{d\_opt}} - \frac{\sqrt{2}}{2}t_2\left(\frac{L_2}{2}\right)$

$f_{\text{d\_max}} = f_{\text{d\_opt}} + \frac{\sqrt{2}}{2}t_2\left(\frac{L_2}{2}\right)$

$f_{\text{s\_min}} = f_{\text{s\_opt}} - \frac{\sqrt{2}}{2}t_1\left(\frac{L_1}{2}\right)$

$f_{\text{s\_max}} = f_{\text{s\_opt}} + \frac{\sqrt{2}}{2}t_1\left(\frac{L_1}{2}\right)$

$f_{\text{d\_min}} \leq f_d \leq f_{\text{d\_max}}$

$f_{\text{s\_min}} \leq f_s \leq f_{\text{s\_max}}$

The spatial and Doppler frequencies of the atom are determined, and a reduction. dictionary is constructed.

5. Simulation Results

The performance of the proposed GS-SR-STAP algorithm was analyzed by simulation experiments and compared with the MDC-SR-STAP [28] and LMSSE-STAP [29] algorithms. All experimental results denoted the average values of 100 independent Monte Carlo simulations. The simulation parameters of the radar system with a side-looking uniform linear array are shown in Table 1.

Table 1. Simulation parameters of the radar system with a side-looking uniform linear array.

Parameter	Value
Element number	10
Pulse number	10
Element spacing (m)	0.15
Operating wavelength (m)	0.3
Airplane velocity (m/s)	240
Aircraft height (m)	3000
Pulse repetition frequency (Hz)	4000
μ_d	4
μ_s	4
Training snapshot number	20

5.1. Space-Time Power Spectrum Analysis of Clutter

The first experiment analyzed the clutter power spectrum of the MDC-SR-STAP, LMSSE-STAP, and GS-SR-STAP algorithms, and the obtained results are shown in Figure 9. In Figure 9a,b, it can be seen that the clutter spectrum estimated by the MDC-SR-STAP and LMSSE-STAP algorithms had an obvious broadening phenomenon, and the clutter energy was dispersed. Thus, these two algorithms were significantly affected by the grid mismatch, which led to a decline in the clutter suppression performance. The clutter spectrum calculated by the GS-SR-STAP algorithm is shown in Figure 9c, where it can be seen that it showed no broadening phenomenon, and the clutter energy was concentrated on the clutter ridge. Therefore, the proposed GS-SR-STAP algorithm achieved better clutter spectrum estimation accuracy than the MDC-SR-STAP and LMSSE-STAP algorithms, which could be beneficial to the improvement of clutter suppression performance.

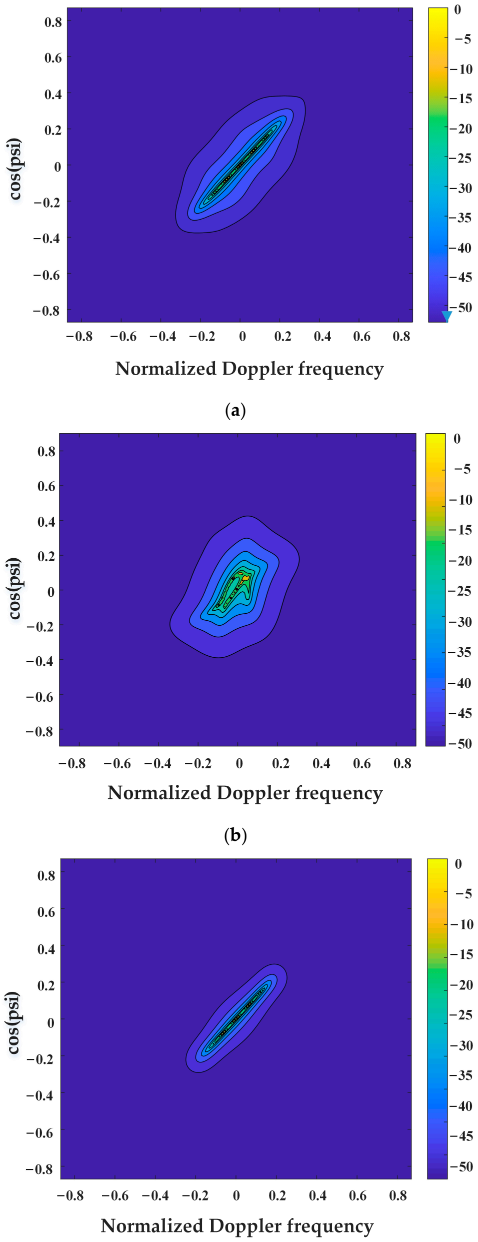

Figure 9. Clutter power spectra. (**a**) MDC-SR-STAP algorithm; (**b**) LMSSE-STAP algorithm; (**c**) GS-SR-STAP algorithm.

5.2. Signal-to-Clutter-Plus-Noise-Ratio Loss Analysis

The second experiment compared the signal-to-clutter-plus-noise-ratio loss ($SCNR_{Loss}$) of the MDC-SR-STAP, LMSSE-STAP, and GS-SR-STAP algorithms to evaluate their clutter suppression performances. The $SCNR_{Loss}$ was calculated as follows:

$$SCNR_{Loss} = \frac{{\sigma_n}^2 \left| {w_{OPT}}^H V_{target} \right|^2}{NK {w_{OPT}}^H \hat{R}_x w_{OPT}} \tag{32}$$

where ${\sigma_n}^2$ is the noise power.

The experimental results are shown in Figure 10, where it can be observed that the notches of the $SCNR_{Loss}$ curves of the MDC-SR-STAP and LMSSE-STAP algorithms were wide, while that of the proposed GS-SR-STAP algorithm was significantly narrower compared to the other two. Also, for the proposed algorithm, a deeper depression was formed in the main clutter region, which was approximately 7 dB and 30 dB deeper than those of the MDC-SR-STAP and LMSSE-STAP algorithms, respectively. Moreover, the $SCNR_{Loss}$ in the sidelobe clutter region of the proposed algorithm was very small. Thus, compared to the other two algorithms, the proposed GS-SR-STAP algorithm had better clutter-suppressing and detection performances for low-speed moving targets.

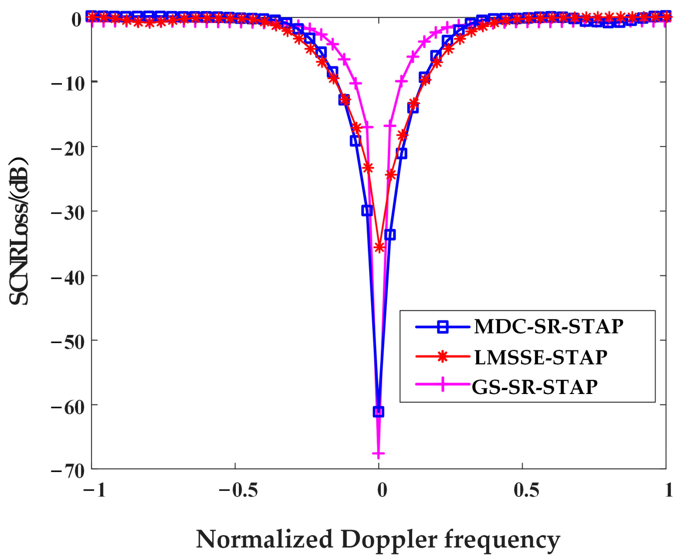

Figure 10. $SCNR_{Loss}$ curves of the MDC-SR-STAP algorithm, LMSSE-STAP algorithm, and GS-SR-STAP algorithm.

5.3. Output Power Analysis

The third experiment analyzed the moving target detection performance of the three algorithms, where each algorithm filtered the snapshot data from 150 range cells. The obtained output power results are shown in Figure 11, where it can be seen that all algorithms could detect the moving target at the 101st range cell. However, compared to the other two algorithms, the residual clutter output power of the LMSSE-STAP algorithm was significantly higher, the output signal-to-noise ratio was lower, and the filtering performance was relatively weak. The residual clutter output power of the GS-SR-STAP algorithm was approximately 15 dB and 25 dB lower than those of the MDC-SR-STAP and LMSSE-STAP algorithms, respectively; thus, the moving target detection performance of the GS-SR-STAP algorithm was the best among all algorithms.

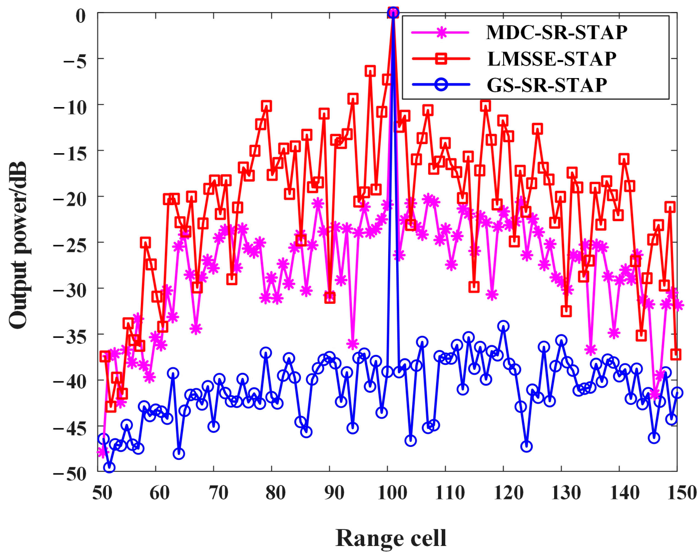

Figure 11. Output power results of the MDC-SR-STAP algorithm, LMSSE-STAP algorithm and GS-SR-STAP algorithm.

5.4. Computational Complexity Analysis

The fifth experiment analyzes and compares the average computational complexity of a single sample of the MDC-SR-STAP algorithm, the LMSSE-STAP algorithm, and the GS-SR-STAP algorithm proposed in this paper, as shown in Table 2, where $\hat{Z} = \mu_d \mu_s$, $Z = NM$.

Table 2. Comparison of average complexity of single sample.

Algorithm Name	Complex Multiplication Number
MDC-SR-STAP	$(12\hat{Z} + 9)\ Z^3 + (8\hat{Z} + 38)\ Z^2 + 18Z$
LMSSE-STAP	$3\hat{Z}Z^3 + (2\hat{Z} + 36)\ Z^2 + 18Z$
GS-SR-STAP	$(12\hat{Z} + 9)\ Z^3 + (8\hat{Z} + 16Z^2) + 6Z$

The MDC-SR-STAP algorithm has the most complex multiplications, and the GS-SR-STAP algorithm has $22Z^2 + 12Z$ fewer complex multiplications than the MDC-SR-STAP algorithm. Although the computational complexity of the two algorithms is higher than that of the LMSSE-STAP algorithm, in comparison, when the computational complexity of the GS-SR-STAP algorithm is less than that of the MDC-SR-STAP algorithm, the GS-SR-STAP algorithm can obtain higher clutter space-time spectrum sparse recovery accuracy and better clutter suppression performance than the MDC-SR-STAP algorithm and the LMSSE-STAP algorithm. Therefore, the algorithm proposed in this paper is more suitable for the requirements of engineering applications.

6. Conclusions

In this paper, a reduced sparse dictionary reconstruction algorithm based on the grid selection is proposed to solve the problem of grid mismatch. First, the atoms most related to the clutter subspace are selected from the traditional sparse recovery dictionary using the spectral value dimension reduction method, and a local search is performed on the region where the initially selected clutter atoms are positioned. By comparing the power spectrum values of the atoms at the vertices of the local grid cell, an approximate position of the optimal atom in the current region is obtained, and the search area is determined by the power spectrum values of the two atoms that are second only to the optimal atom. Notably, the power spectrum values considered are only those of the optimal atom and the two adjacent atoms when arranged according to the power spectrum. The grid spacing is gradually refined, and the search area is narrowed until the full iteration termination condition is satisfied. The optimal atom's location is determined, and a division method of discrete grids along the parallel and vertical directions of the clutter ridge is employed to construct a local reduction dictionary. In this way, a more accurate clutter power spectrum is obtained to calculate the CCMs and improve the clutter suppression performance. The proposed algorithm is verified by simulation experiments and compared with MDC-SR-STAP and LMSSE-STAP algorithms. The results show that the proposed algorithm can find the atoms that match the real clutter points more accurately than the other two algorithms. Compared with the traditional dictionary, the dictionary constructed in this study reduces the influence of the dictionary mismatch effect, improving clutter suppression performance and algorithm practicability. This leads to better STAP performance in the case of side-looking. However, in non-side-looking scenarios, the clutter ridge takes the form of a curve in the space-time plane, leading to a serious grid misalignment phenomenon. Therefore, the main focus of the next step is to explore a dictionary correction algorithm for non-side-looking cases.

Author Contributions: Conceptualization, Z.G. and C.Z.; methodology, C.Z.; software, C.Z.; validation, Z.G. and C.Z.; formal analysis, Z.G.; investigation, Z.G., C.Z. and P.H.; resources, Z.G. and C.Z.; data curation, Z.G. and C.Z.; writing—original draft preparation, C.Z.; writing—review and editing, Z.G. and P.H.; visualization, C.Z.; supervision, W.X. and W.T.; project administration, Z.G. and P.H.; funding acquisition, Z.G. and P.H. All authors have read and agreed to the published version of the manuscript.

Funding: This research was funded by National Natural Science Foundation of China under grant number 61761037 and number 62071258, the Natural Science Foundation of Inner Mongolia under grant number 2021MS06005 and number 2020ZD18, the Basic Scientific Research Business Cost Project of Colleges directly under the Inner Mongolia under grant number JY20220147.

Data Availability Statement: Data is contained within the article.

Conflicts of Interest: The authors declare no conflicts of interest.

References

1. Xie, W.; Duan, K.; Wang, Y. Space time adaptive processing technique for airborne radar: An overview of its development and prospects. *J. Radars* **2017**, *6*, 575–586.
2. Duan, K.; Xu, H.; Yuan, H.; Xie, H.; Wang, Y. Reduced-DOF three-dimensional STAP via subarray synthesis for nonsidelooking planar array airborne radar. *IEEE Trans. Aerosp. Electron. Syst.* **2019**, *56*, 3311–3325. [CrossRef]
3. Sun, K.; Zhang, H.; Li, G.; Meng, H.; Wang, X. STAP via sparse Recovery of Clutter Spectrum. *Tien Tzu Hsueh Pao/Acta Electron. Sin.* **2011**, *39*, 1389–1393.
4. Wang, T. *Study of Simplified STAP and Its Application to Airborne Radar*; Research Paper; Xidian University: Xi'an, China, 2001.
5. Yang, Z.; Li, X.; Wang, H. An overview of space-time adaptive processing technology based on sparsity of space-time power spectrum. *Acta Electron. Sin.* **2014**, *42*, 1194.
6. Duan, K.Q.; Wang, Z.T.; Xie, W.C.; Gao, F.; Wang, Y.L. A space-time adaptive processing algorithm based on joint sparse recovery. *J. Radars* **2014**, *3*, 229–234. [CrossRef]
7. Wang, Y.; Chen, J.; Bao, Z.; Peng, Y. Robust space-time adaptive processing for airborne radar in nonhomogeneous clutter environments. *IEEE Trans. Aerosp. Electron. Syst.* **2003**, *39*, 70–81. [CrossRef]
8. Ding, Q.; Wang, Y.; Zhang, Y. Research on Algorithms for Reduced Rank Adaptive Filtering. *Radar Sci. Technol.* **2005**, *4*, 232–239.
9. Zhang, W.; He, Z.; Li, J.; Liu, H.; Sun, Y. A method for finding best channels in beam-space post-Doppler reduced-dimension STAP. *IEEE Trans. Aerosp. Electron. Syst.* **2014**, *50*, 254–264. [CrossRef]
10. Honig, M.L.; Goldstein, J.S. Adaptive reduced-rank interference suppression based on the multistage Wiener filter. *IEEE Trans. Commun.* **2002**, *50*, 986–994. [CrossRef]
11. De Lamare, R.C.; Wang, L.; Fa, R. Adaptive reduced-rank LCMV beamforming algorithms based on joint iterative optimization of filters: Design and analysis. *Signal Process.* **2010**, *90*, 640–652. [CrossRef]
12. Melvin, W.L.; Showman, G.A. An approach to knowledge-aided covariance estimation. *IEEE Trans. Aerosp. Electron. Syst.* **2006**, *42*, 1021–1042. [CrossRef]
13. Zhang, T. *Airborne MIMO Radar Clutter Suppression Based on Sparse Recovery*; Research Paper; Nanjing University of Aeronautics and Astronautics: Nanjing, China, 2018.
14. Lesicka, A.; Kawalec, A. An application of the orthogonal matching pursuit algorithm in space-time adaptive processing. *Sensors* **2020**, *20*, 3468. [CrossRef]

15. Deng, J. *Research on Compressive Sensing Signal Reconstruction by Convex Optimization*; Research Paper; Harbin Institute of Technology: Harbin, China, 2011.
16. Sun, K.; Meng, H.; Wang, Y.; Wang, X. Direct data domain STAP using sparse representation of clutter spectrum. *Signal Process.* **2011**, *91*, 2222–2236. [CrossRef]
17. Duan, K.; Wang, Z.; Xie, W.; Chen, H.; Wang, Y. Sparsity-based STAP algorithm with multiple measurement vectors via sparse Bayesian learning strategy for airborne radar. *IET Signal Process.* **2017**, *11*, 544–553. [CrossRef]
18. Duan, K.; Liu, W.; Duan, G.; Wang, Y. Off-grid effects mitigation exploiting knowledge of the clutter ridge for sparse recovery STAP. *IET Radar Sonar Navig.* **2018**, *12*, 557–564. [CrossRef]
19. Li, Z.; Wang, T. ADMM-based low-complexity off-grid space-time adaptive processing methods. *IEEE Access* **2020**, *8*, 206646–206658. [CrossRef]
20. Zhang, T.; Hu, Y.; Lai, R. Gridless super-resolution sparse recovery for non-sidelooking STAP using reweighted atomic norm minimization. *Multidimens. Syst. Signal Process.* **2021**, *32*, 1259–1276. [CrossRef]
21. Zhang, T.; Guo, J.; Lai, R. Gridless Sparse Recovery for Non-sidelooking Space-Time Adaptive Processing Based on Atomic Norm Minimization. *J. Electron. Inf. Technol.* **2021**, *43*, 1235–1242.
22. Yuan, H.; Xu, H.; Duan, K.; Xie, W.; Liu, W.; Wang, Y. Sparse Bayesian learning-based space-time adaptive processing with off-grid self-calibration for airborne radar. *IEEE Access* **2018**, *6*, 47296–47307. [CrossRef]
23. Cui, W.; Wang, T.; Wang, D.; Liu, K. An efficient sparse Bayesian learning STAP algorithm with adaptive Laplace prior. *Remote Sens.* **2022**, *14*, 3520. [CrossRef]
24. Cui, W.; Wang, T.; Wang, D.; Zhang, X. A novel sparse recovery-based space-time adaptive processing algorithm based on gridless sparse Bayesian learning for non-sidelooking airborne radar. *IET Radar Sonar Navig.* **2023**, *17*, 1380–1390. [CrossRef]
25. He, T.; Tang, B.; Zhang, J.; Zhang, Y. MIMO STAP sparse dictionary construction method under off-grid condition. *J. Detect. Control* **2020**, *42*, 106–111.
26. He, P.; He, S.; Yang, Z.; Huang, P. An off-grid STAP algorithm based on local mesh splitting with bistatic radar system. *IEEE Signal Process. Lett.* **2020**, *27*, 1355–1359. [CrossRef]
27. Zhang, Y.; Jin, Y.; Chen, S.; Wu, Y.; Hao, C. A robust STAP algorithm using two prior knowledge. *Signal Process.* **2022**, *38*, 1367–1379.
28. Wang, Z.; Xie, W.; Duan, K.; Wang, Y. Clutter suppression algorithm based on fast converging sparse Bayesian learning for airborne radar. *Signal Process.* **2017**, *130*, 159–168. [CrossRef]
29. Melvin, W.L.; Guerci, J.R. Knowledge-aided signal processing: A new paradigm for radar and other advanced sensors. *IEEE Trans. Aerosp. Electron. Syst.* **2006**, *42*, 983–996. [CrossRef]
30. Cui, N.; Xing, K.; Yu, Z.; Duan, K. Tensor-based sparse recovery space-time adaptive processing for large size data clutter suppression in airborne radar. *IEEE Trans. Aerosp. Electron. Syst.* **2022**, *59*, 907–922. [CrossRef]
31. Xu, W.; Gao, Z.; Xu, W.; Huang, P.; Tan, W. Space-time adaptive processing with dictionary calibration based on iterative adaptive approach. *J. Signal Process.* **2021**, *37*, 2216–2226.
32. Li, Z.; Zhang, Y.; He, X.; Guo, Y. Low-complexity off-grid STAP algorithm based on local search clutter subspace estimation. *IEEE Geosci. Remote Sens. Lett.* **2018**, *15*, 1862–1866. [CrossRef]